SCIENCE CHINA
Earth Sciences

• RESEARCH PAPER •

September 2011 Vol.54 No.9: 1394–1399
doi: 10.1007/s11430-011-4262-6

Equation of state of CAS phase to pressure of the uppermost lower mantle at ambient temperature

LIU Xi[1*], HE Qiang[1], DENG LiWei[1,2], ZHAI ShuangMeng[1], HU XiaoMin[1], LI BaoSheng[3], ZHANG LiFei[1], CHEN ZhiQiang[4] & LIU Qiong[1]

[1]*Key Laboratory of Orogenic Belts and Crustal Evolution, MOE; School of Earth and Space Sciences, Peking University, Beijing 100871, China;*
[2]*Geophysical Laboratory and Center for High-pressure Research, Carnegie Institution of Washington, 5251 Broad Branch Road NW, Washington DC, 20015-1305, USA;*
[3]*Mineral Physics Institute, State University of New York, Stony Brook, New York 11794, USA;*
[4]*National Synchrotron Light Source, Brookhaven National Laboratory, Upton, New York 11973, USA*

Received December 14, 2010; accepted June 29, 2011

The CAS phase is a major constituent phase for the continental crust and basaltic compositions at the *P-T* conditions of the Earth's mantle, and potentially plays an important role in the geodynamic processes related to slab subduction. Its equation of state has been investigated here at ambient temperature up to about 25 GPa by using a diamond-anvil cell and synchrotron X-ray radiation. Its *P-V* data, fitted to the third-order Birch-Murnaghan equation, yield an isothermal bulk modulus (K_T) of 185 (9) GPa and first pressure derivative (K_T') of 7.2 (12). If K_T' is fixed at 4, the derived K_T is 212 (4) GPa. Additionally, the CAS phase is strongly elastically anisotropic, with its *a*-axis direction much less compressible than *c*-axis direction: $K_{T\text{-}a}$: $K_{T\text{-}c}$ = 2.19.

anisotropic elasticity, CAS phase, equation of state, synchrotron X-ray radiation

Citation: Liu X, He Q, Deng L W, et al. Equation of state of CAS phase to pressure of the uppermost lower mantle at ambient temperature. Sci China Earth Sci, 2011, 54: 1394−1399, doi: 10.1007/s11430-011-4262-6

A CaO-, Al_2O_3- and SiO_2-rich phase (CAS) was observed by Irifune et al. [1] when they experimentally investigated the phase relationships of the continental crust composition at pressures of the mantle of the Earth. Subsequently the CAS phase was compositionally and structurally constrained in the system $CaO\text{-}Al_2O_3\text{-}SiO_2$ [2–5], with its composition close to $CaAl_4Si_2O_{11}$ and its structure of $P6_3/mmc$. Later this phase was observed in the high-*P* experiments using the basaltic compositions as the starting materials, although its composition was slightly different to $CaAl_4Si_2O_{11}$ [6–8]. According to recent high-*P* experimental exploration [9–11], the CAS phase is stable from about 10 to about 30 GPa. On the other hand, the CAS also occurs as a natural mineral, and has been identified in shocked Martian meteorites [12].

Both continental crust material and basaltic material could be subducted to great depths of the Earth along the subduction zone, and later either be digested by the surrounding mantle material to create some compositional heterogeneity in the mantle [13] or be quickly exhumed to the surface of the Earth [14–16]. Obviously, this dynamic process is largely dependent on the equations of states (EoS) of the constituent phases of the continental crust/basaltic material and the mantle composition. As one of the involved phases, the CAS phase might be important to this process. However, the knowledge of the CAS phase at high pressures has not been satisfactory, and the EoS of this phase

*Corresponding author (email: xi.liu@pku.edu.cn)

has been investigated only in one experimental study [17]. Even in that experimental investigation [17], no *P-V* data were reported from 0 to about 16 GPa, leaving the EoS not well constrained. Here we synthesized the CAS phase in the system CaO-Al_2O_3-SiO_2 with a multi-anvil (MA) press, and investigated its EoS from 0 to about 25 GPa with a diamond-anvil cell (DAC) and synchrotron X-ray radiation.

1 Experimental details

The CAS phase of the composition $CaAl_4Si_2O_{11}$ was synthesized at 20 GPa and 1400°C with a 5000-ton Kawai-type double-stage uniaxial split-sphere MA press installed at the Institute for Study of the Earth's Interior, Okayama University (Run-1472) [18]. The experimental details were given in Xue et al. [18]. The experimental product contained the CAS phase only, with its composition and structure confirmed by electron microprobe analyses and powder XRD, respectively. This material was mixed with a small amount of Au powder, and then used as the starting material in the compression experiments with the DAC.

With a symmetrical DAC, we conducted in situ high-pressure angle dispersive X-ray powder diffraction experiments at the beamline X17C, National Synchrotron Light Source, Brookhaven National Laboratory. We used T301 stainless steel plates as the gaskets and a 4∶1 methanole-thanol mixture as the pressure medium. In order to determine the experimental pressure by the ruby fluorescence method [19], we loaded with the sample a couple of tiny ruby balls. The experimental pressure was also estimated using the EoS of Au [20], but the quality of the pressure estimates with this method was generally low (see later discussion). An online CCD detector was used to collect the X-ray diffraction patterns, and the data-collecting time was 20 minutes. The X-ray diffraction patterns were later processed with the Fit2D program to generate the conventional one-dimension profile [21]. These high-*P* experimental and data-processing techniques have been well established and used in our previous experimental investigations [22–26]. The hexagonal unit-cell parameters of the CAS phase at different pressures were calculated by refining the unit cells using the strongest diffraction peaks 101, 102, 004, 110, 104, 112, 202, 203, 206, 214 and 302, whose positions were determined by a full spectrum refinement of the powder X-ray patterns. The unit-cell parameters of Au were derived using the reflections 111, 200 and 220.

2 Result and discussion

We conducted the compression experiments up to about 44 GPa at ambient temperature, and did not observe any phase transition, which is in good agreement with the result of Ono et al. [17]. Although the pressure media of the 4∶1 methanol-ethanol mixture solidified at about 10 GPa [27], no significant peak-broadening of the X-ray diffraction patterns was observed for the high-*P* experiments up to approximately 25 GPa. Consequently, we report in this paper the *P-V* data up to this pressure only. Peak-indexing of the high-*P* powder X-ray diffraction patterns of the CAS phase has been done and shown in Figure 1, according to the single crystal X-ray diffraction data in Gautron et al. [4]. Typical powder X-ray diffraction patterns for the CAS phase are illustrated in Figure 2. From these X-ray diffraction patterns, we can see that the Au peaks have some general problems which strongly affect their accurate peak-position

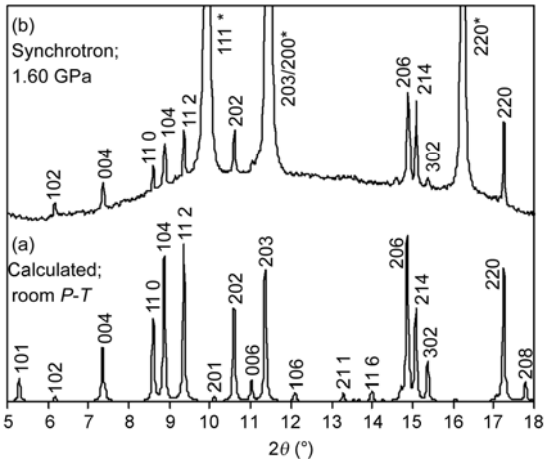

Figure 1 Indexing the X-ray diffraction patterns. (a) Pattern calculated from the data in ref. [4]; (b) synchrotron data collected at 1.60 GPa. Peaks for Au are denoted by the asterisks. Wave length is 0.4066 Å.

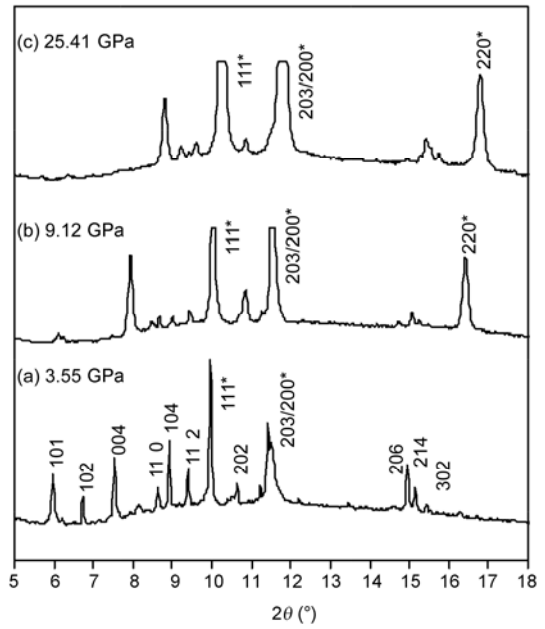

Figure 2 Representative X-ray diffraction patterns of the CAS phase at 3.55 GPa (a), 9.12 GPa (b) and 25.41 GPa (c). Peaks for Au are denoted by the asterisks. As pressure increases, the diffraction peaks of the CAS phase become weaker.

determination: peak 111 occurs at low 2θ angle so that its position bears relatively low accuracy, peak 200 overlaps with the peak 203 of the CAS phase, and peak 220 is sometimes absent. As a result, the pressures estimated by using the Au EoS [20] are much less interconsistent than those estimated by using the ruby florescent method [19]. In our later discussion, therefore, we only use the pressures estimated by the ruby florescent method. The unit-cell parameters at different pressures derived from the X-ray diffraction patterns are listed in Table 1, and graphed in Figure 3.

High pressure reduces the size of the unit cell of the CAS phase (Figure 3). For the investigated pressure interval, the reduction of the lattice parameters a and c with pressure is apparently non-linear, and can be empirically described as: a=5.432(2)–0.0065(4)P+0.00004(2)P^2 and c=12.708(8)–0.0291(17)P+0.00026(6)P^2 with a and c in Å and P in GPa.

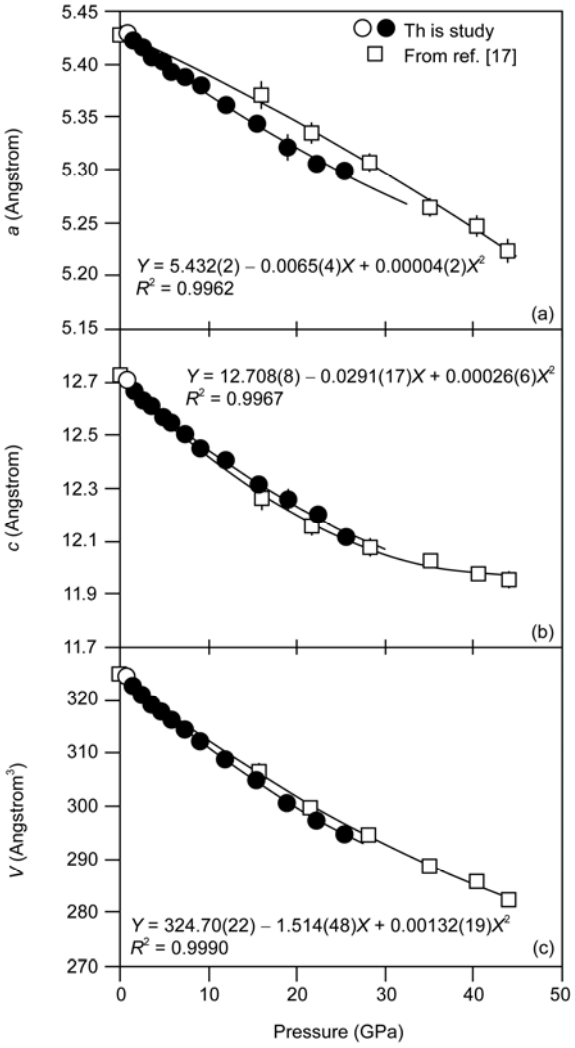

Figure 3 Pressure dependence of the unit-cell parameters of the CAS phase. (a) a-axis; (b) c-axis; (c) volume. Filled circles represent data collected during compression whereas empty circle represents data collected during decompression. The data from ref. [17] are shown for comparison. Thick curves represent empirical fittings to our data, as described by the equations.

Table 1 Unit-cell parameters of the CAS phase at different pressures

P_1 (GPa)[a)]	P_2 (GPa)[b)]	a (Å)	c (Å)	V (Å^3)	a/c
0.0001[c)]	0.0001	5.428 (4)[d)]	12.728 (26)	324.7 (8)	0.426 (1)
0.72 (7)[e)]	0.70	5.429 (2)	12.703 (11)	324.28 (23)	0.427 (0)
1.60 (3)	1.98	5.421 (1)	12.667 (4)	322.37 (12)	0.428 (0)
2.53 (8)	2.92	5.416 (1)	12.629 (5)	320.83 (10)	0.429 (0)
3.55 (5)	3.65	5.406 (1)	12.607 (3)	319.02 (7)	0.429 (0)
4.72 (8)	4.91	5.403 (1)	12.566 (2)	317.67 (7)	0.430 (0)
5.75 (0)	6.86	5.393 (1)	12.547 (6)	315.96 (14)	0.430 (0)
7.40 (13)	7.07	5.388 (2)	12.503 (11)	314.28 (27)	0.431 (0)
9.12 (12)	8.46	5.380 (4)	12.450 (18)	312.08 (45)	0.432 (1)
11.91 (14)	11.21	5.361 (4)	12.406 (17)	308.72 (40)	0.432 (1)
15.58 (11)	14.21	5.344 (3)	12.319 (15)	304.70 (34)	0.434 (1)
19.03 (16)	16.28	5.321 (12)	12.260 (39)	300.6 (12)	0.434 (2)
22.24 (5)	21.32	5.306 (3)	12.204 (14)	297.50 (32)	0.435 (1)
25.41(28)	25.95	5.298 (3)	12.119 (16)	294.64 (36)	0.437 (1)

a) Pressure determined by the ruby fluorescence method [19]; b) pressure determined by the EoS of Au [20]; c) data from ref. [17], collected after decompression; d) number in parentheses representing one standard deviation in the rightmost digit; e) data collected during decompression.

Similarly, the dependence of the volume on pressure can be empirically fitted as: V = 324.70(22)–1.514(48)P+0.0132 (19) P^2 with V in Å^3 and P in GPa. Figure 3 shows that the result of this investigation is much comparable to that in Ono et al. [17], with the largest difference associated with the a-axis: the a-P curve from this study is concave up while that from Ono et al. [17] concave down (Figure 3(a)). In addition, Figure 3 shows that the reduction rate of the unit-cell volume by pressure determined in this study is faster than that determined in Ono et al. [17] (Figure 3(c)), which should lead to a smaller bulk modulus.

The evolution with pressure of the a/c ratios of the CAS phase was not constrained by the data of Ono et al. [17] (Figure 4). Our data, on the other hand, clearly show a rapid increase of the a/c ratio with pressure, indicating the linear compressibility of the CAS is significantly anisotropic for the pressure range investigated in our study.

In order to determine the isothermal bulk modulus, the P-V data of the CAS phase have been fitted to the third-order Birch-Murnaghan equation of state (BM-EoS) by a least-squares method [28]:

$$P = 3K_T f_E (1+2f_E)^{\frac{5}{2}}\left[1+\frac{3}{2}(K_T'-4)f_E\right],$$

where P is the pressure, K_T the isothermal bulk modulus, K_T' the first pressure derivative of K_T, and f_E the Eulerian definition of finite strain, which is $[(V_0/V)^{2/3}-1]/2$, respectively. In the Eulerian definition of finite strain, V_0 is the volume at zero pressure whereas V is the volume at high pressure. When K_T' is set as 4, the isothermal bulk modulus (K_T) of the CAS phase is 212 (4) GPa, and the zero-pressure volume is 324.52 (15) Å^3. If K_T' is not fixed, the results of our best data-fitting are K_T = 185 (9) GPa,

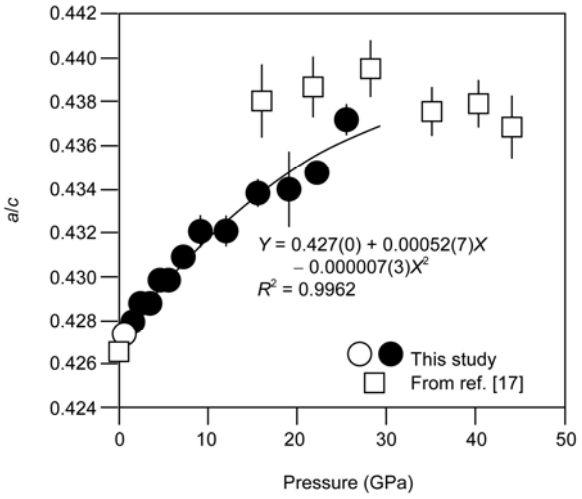

Figure 4 Correlation of the *a*/*c* ratio of the CAS phase and pressure. Filled circles represent data collected during compression whereas empty circle represents datum collected during decompression. The data from ref. [17] are shown for comparison. Thick curve represents an empirical fitting to our data, as described by the equation.

K_T' = 7.2 (12) and V_0 = 325.05 (22) Å^3. In contrast, the results from Ono et al. [17] were K_T = 239 (8) GPa and V_0 = 324.63 (77) Å^3 (K_T' = 4), or K_T = 227 (29) GPa, K_T' = 4.8(20) and V_0 = 324.72(79) Å^3. It follows that the bulk modulus of the CAS phase determined in our study is about 10% smaller than that determined by Ono et al. [17] (K_T' set as 4).

As mentioned earlier, the pressure media in our compression experiments solidified at about 10 GPa so that complete hydrostatic conditions could not be met in the experiments at higher pressures. Although we did not see apparent peak-broadening in the X-ray diffraction patterns collected at pressures above 10 GPa (Figure 2), it is still necessary to do some checking. The *P*-*V* data collected in the experiments at P < 10 GPa have been fitted to the third-order BM-EoS, yielding K_T = 195 (8) GPa and V_0 = 324.93 (24) Å^3 (K_T' = 4). These values agree very well with the results derived from the whole datum set (K_T = 212 (4) GPa and V_0 = 324.52 (15) Å^3 with K_T' set as 4), suggesting that nonhydrostatic condition was fortunately not a big issue in our experiments at P > 10 GPa. On the other hand, the experiments done by Ono et al. [17], which suggested K_T = 239 (8) GPa and V_0 = 324.63 (77) Å^3 (K_T' = 4), might have been affected by deviatoric stress in the DAC although they used a laser to heat the sample. According to He et al. [29], nonhydrostatic condition in the DAC experiments should lead to larger bulk modulus if the sample is probed by an X-ray that is positioned parallel to the loading direction of the DAC; this was the experimental setup used in Ono et al. [17] and this study. Alternatively, the potential 10% overestimation of the K_T in Ono et al. [17] might be readily explained by the lacking of *P*-*V* data in the pressure interval of 0–16 GPa.

A linearized third-order BM-EoS [30] was used to obtain the parameters of the equations of state for the crystallographic axes, yielding: a_0 = 5.432 (2) Å, $K_{T\text{-}a}$ = 256 (21) GPa and $K'_{T\text{-}a}$ = 7.0 (24) for the *a*-axis while c_0 = 12.721(6) Å, $K_{T\text{-}c}$ = 117(8) GPa and $K'_{T\text{-}c}$ = 6.3 (11) for the *c*-axis. The elastic anisotropy ($K_{T\text{-}a}$:$K_{T\text{-}c}$) of the CAS phase, therefore, is about 2.19; in other words, the *a*-axis direction is much less compressible than the *c*-axis direction.

The quality of the derived third-order Birch-Murnaghan equations of state for the CAS phase can be evaluated by using the f_E-F plot (Figure 5); F is defined as $F \equiv P/[3f_E(1+2f_E)^{5/2}]$. Using F, the third-order BM-EoS can be rewritten as:

$$F = K_T + 3/2K_T(K_T' - 4)f_E,$$

so that the slope of the line defined by the experimental data should be equal to $3/2K_T(K_T' - 4)$, and the intercept value is the isothermal bulk modulus. Accordingly, a slope of zero means K_T' = 4, a negative slope K_T' < 4, and a positive slope K_T' > 4. Figure 5(a) clearly suggests that the K_T' of the phase CAS is larger than 4, in agreement with our *P*-*V* data-fitting results detailed above. Similarly, the quality of the derived third-order BM-EoS for the axes of the CAS phase has been evaluated by using the f_E-F plot (Figure 5(b) and (c)).

For the continental crust and sediment compositions, many phases including the CAS phase are stable at the *P*-*T* conditions of the mantle [1, 32]. The compressibility of the CAS has been compared in Figure 6 to that of coesite (Coe; SiO_2) [33], omphacitic clinopyroxene (Cpx) [34], majoritic pyrope (Mj-Py; $Mj_{38}Py_{62}$) [35], grossular (Gro; $Ca_3Al_2Si_3O_{12}$) [36], phase Egg (Egg; $AlSiO_3OH$) [37], $KAlSi_3O_8$-hollandite (K-Holl-I; $KAlSi_3O_8$) [38], $NaAlSiO_4$-CF (CF; $NaAlSiO_4$) [39], kyanite (Ky; Al_2SiO_5) [23], calcium perovskite (CaPv; $CaSiO_3$) [40], corundum (Cor; Al_2O_3) [41], phase δ-AlOOH (AlOOH) [42], and Al_2O_3-bearing stishovite (St; SiO_2) [43]. Two points should be pointed out in Figure 6. Firstly, our present EoS investigation suggests that the CAS is more compressible, or denser in other words, than previously determined [17]. Secondly, the compressibility of the anhydrous silicate phases generally decreases with the increase of the Si atom-coordination number (for example 4 in Coe or 6 in St). From this perspective, the compressibility of the CAS phase obtained by Ono et al. [17] seems too small because its V/V_0-P curve is well located in the area for the phases with their Si atoms in 6-fold coordination; some of the Si atoms in the CAS are 4-fold coordinated while some are 6-fold coordinated [4, 5, 18]. This argument apparently favours our experimental result.

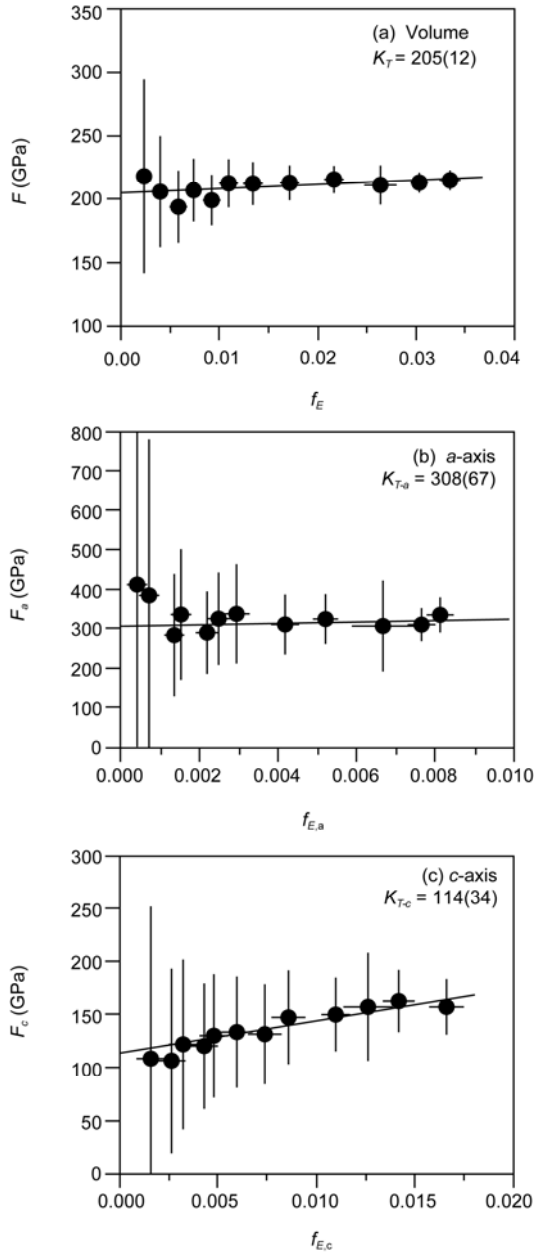

Figure 5 Eulerian strain-normalized pressure (f_E-F) plot of the CAS phase. (a) Volume; (b) a-axis; (c) c-axis. Estimated standard deviations have been calculated according to the method in ref. [31]. The solid lines are the weighted linear fit through the data at $P > 1$ GPa. The data at 1 atm from ref. [17], with large uncertainties, were used in the calculation, which led to overestimated standard deviations.

3 Conclusions

In this study we carried out, at ambient temperature and up to 25 GPa, in situ synchrotron X-ray diffraction experiments with the DAC to determine the EoS of the CAS phase. The isothermal bulk modulus of the CAS is 185(9) GPa, and its first pressure derivative is 7.2 (12). If the first pressure derivative of the isothermal bulk modulus is fixed at 4, the derived isothermal bulk modulus is 212 (4) GPa. Moreover, the CAS phase is strongly elastically anisotropic, with its a-axis direction much less compressible than c-axis direction: $K_{T\text{-}a}$:$K_{T\text{-}c}$ = 2.19.

Figure 6 Comparison of the EoS of the phases related to the continental crust/sediment compositions at the P-T conditions of the mantle. The number following the name of the phase is the coordination number of the Si atom.

This study was financially supported by National Natural Science Foundation of China (Grant Nos. 40872033, 40821002), and Fundamental Research Funds for the Central Universities to Liu Xi. We thank the anonymous reviewers for their constructive comments which greatly improved our manuscript.

1 Irifune T, Ringwood A E, Hibberson W O. Subduction of continental crust and terrigenous and pelagic sediments: An experimental study. Earth Planet Sci Lett, 1994, 126: 351–368
2 Gautron L, Kesson S E, Hibberson W O. Phase relations for $CaAl_2Si_2O_8$ (anorthite composition) in the system CaO-Al_2O_3-SiO_2 at 14 GPa. Phys Earth Planet Inter, 1996, 97: 71–81
3 Gautron L, Fitz Gerald J D, Kesson S E, et al. Hexagonal Ba-ferrite: A good model for the crystal structure of a new high-pressure phase $CaAl_4Si_2O_{11}$? Phys Earth Planet Inter, 1997, 102: 223–229
4 Gautron L, Angel R J, Miletich R. Structural characterization of the high-pressure phase $CaAl_4Si_2O_{11}$. Phys Chem Minerals, 1999, 27: 47–51
5 Grey I E, Madsen I C, O'Neill H St C, et al. Rietveld refinement of high-pressure $CaAl_4Si_2O_{11}$ with the R-type ferrite structure. N Jb Miner Mh, 1999, 3: 104–112
6 Hirose K, Fei Y, Ma Y, et al. The fate of subducted basaltic crust in the Earth's lower mantle. Nature, 1999, 397: 53–56
7 Wang W, Takahashi E. Subsolidus and melting experiments of a K-rich basaltic composition to 27 GPa: Implication for the behavior of potassium in the mantle. Am Mineral, 1999, 84: 357–361
8 Hirose K, Fei Y. Subsolidus and melting phase relations of basaltic composition in the uppermost lower mantle. Geochim Cosmochim Acta, 2002, 66: 2099–2108
9 Zhai S, Ito E. Phase relations of $CaAl_4Si_2O_{11}$ at high-pressure and high-temperature with implications for subducted continental crust into the deep mantle. Phys Earth Planet Inter, 2008, 167: 161–167
10 Ishibashi K, Hirose K, Sata N, et al. Dissociation of CAS phase in the uppermost lower mantle. Phys Chem Minerals, 2008, 35: 197–200
11 Akaogi M, Haraguchi M, Yaguchi M, et al. High-pressure phase rela-

tions and thermodynamic properties of $CaAl_4Si_2O_{11}$ CAS phase. Phys Earth Planet Inter, 2009, 173: 1–6
12 Beck P, Gillet P, Gautron L, et al. A new natural high-pressure (Na,Ca)-hexaluminosilicate [$(Ca_xNa_{1-x})Al_{3+x}Si_{3-x}O_{11}$] in shocked Martian meteorites. Earth Planet Sci Lett, 2004, 219: 1–12
13 Hofmann A W. Mantle geochemistry: The message from oceanic volcanism. Nature, 1997, 385: 219–229
14 Xu S, Okay A, Ji S, et al. Diamond from the Dabie Shan metamorphic rocks and its implication for tectonic setting. Science, 1992, 256: 80–82
15 Ye K, Cong B, Ye D. The possible subduction of continental material to depths greater than 200 km. Nature, 2000, 407: 734–736
16 Song S G, Su L, Niu Y, et al. Evolution from oceanic subduction to continental collision: A case study of the Northern Tibetan Plateau inferred from geochemical and geochronological data. J Petrol, 2006, 47: 435–455
17 Ono S, Iizuka T, Kikegawa T. Compressibility of the calcium aluminosilicate, CAS, phase to 44 GPa. Phys Earth Planet Inter, 2005, 150: 331–338
18 Xue X, Zhai S, Kanzaki M. Si-Al distribution in high-pressure $CaAl_4Si_2O_{11}$ phase: A ^{29}Si and ^{27}Al NMR study. Am Mineral, 2009, 94: 1739–1742
19 Mao H K, Bell P M, Shaner J W, et al. Specific volume measurements of Cu, Mo, Pt, and Au and calibration of ruby R1 fluorescence pressure gauge for 0.006 to 1 Mbar. J Appl Phys, 1978, 49: 3276–3283
20 Takemura K, Dewaele A. Isothermal equation of state for gold with a He-pressure medium. Phys Rev B, 2008, 78: 104–119
21 Hammersley J. Fit2D report. Europe Synchrotron Radiation Facility, Grenoble, France, 1996
22 Liu X, Shieh S R, Fleet M E, et al. High-pressure study on lead fluorapatite. Am Mineral, 2008, 93: 1581–1584
23 Liu X, Shieh S R, Fleet M E, et al. Compressibility of a natural kyanite to 17.5 GPa. Prog Nat Sci, 2009, 19: 1281–1286
24 Liu X, Shieh S R, Fleet M E, et al. Equation of state of carbonated hydroxylapatite at ambient temperature up to 10 GPa: Significance of carbonate. Am Mineral, 2011, 96: 74–80
25 Zhai S, Liu X, Shieh S R, et al. Equation of state of γ–tricalcium phosphate, γ-$Ca_3(PO_4)_2$, to lower mantle pressures. Am Mineral, 2009, 94: 1388–1391
26 Fleet M E, Liu X, Shieh S R. Structural change in lead fluorapatite at high pressure. Phys Chem Minerals, 2010, 37: 1–9
27 Klotz S, Chervin J C, Munsch P, et al. Hydrostatic limits of 11 pressure transmitting media. J Phys D: Appl Phys, 2009, 42: 075413
28 Birch F. Finite elastic strain of cubic crystals. Phys Rev, 1947, 179: 3065–3072
29 He D, Shieh S R, Duffy T S. Strength and equation of state of boron suboxide from radial X-ray diffraction in a diamond cell under non-hydrostatic compression. Phys Rev B, 2004, 70: 184121
30 Angel R J. Equation of state. In: Hazen R M, Downs R T, eds. High-temperature and High-pressure Crystal Chemistry. Reviews in Mineralogy and Geochemistry, Vol 41. Mineralogical Society of America, Chantilly, Virginia, 2001. 35–60
31 Heinz D L, Jeanloz R. The equation of state of the gold calibration standard. J Appl Phys, 1984, 55: 885–893
32 Rapp R, Irifune T, Shimizu N, et al. Subduction recycling of continental sediments and the origin of geochemically enriched reservoirs in the deep mantle. Earth Planet Sci Lett, 2008, 271: 14–23
33 Angel R J, Mosenfelder J L, Shaw C S J. Anomalous compression and equation of state of coesite. Phys Earth Planet Int, 2001, 124: 71–79
34 Nishihara Y, Takahashi E, Matsukage K, et al. Thermal equation of state of omphacite. Am Mineral, 2003, 88: 80–86
35 Wang Y, Weidner D J, Zhang J, et al. Thermal equation of state of garnets along the pyrope-majorite join. Phys Earth Planet Int, 1998, 105: 59–71
36 Pavese A, Diella V, Pischedda V, et al. Pressure-volume-temperature equation of state of andradite and grossular, by high-pressure and high-temperature powder diffraction. Phys Chem Minerals, 2001, 28: 242–248
37 Vanpeteghem C B, Ohtani E, Kondo T, et al. Compressibility of phase Egg $AlSiO_3OH$: Equation of state and role of water at high pressure. Am Mineral, 2003, 88: 1408–1411
38 Nishiyama N, Rapp R P, Irifune T, et al. Stability and *P-V-T* equation of state of $KAlSi_3O_8$-hollandite determined by in situ X-ray observations and implications for dynamics of subducted continental crust material. Phys Chem Minerals, 2005, 32: 627–637
39 Guignot N, Andrault D. Equations of state of Na-K-Al host phases and implications for MORB density in the lower mantle. Phys Earth Planet Int, 2004, 143/144: 107–128
40 Shim S H, Duffy T, Shen G. The equation of state of $CaSiO_3$ perovskite to 108 GPa at 300 K. Phys Earth Planet Int, 2000, 120: 327–338
41 d'Amour H, Schiferl D, Denner W, et al. High-pressure single-crystal structure determinations for ruby up to 90 kbar using an automatic diffractometer. J Appl Phys, 1978, 48: 4411–4416
42 Vanpeteghem C B, Ohtani E, Kondo T. Equation of state of the hydrous phase δ-AlOOH at room temperature up to 22.5 GPa. Geophys Res Lett, 2002, 29: 23–25
43 Ono S, Suto T, Hirose K, et al. Equation of state of Al-bearing stishovite to 40 GPa at 300 K. Am Mineral, 2002, 87: 1486–1489